https://doi.org/10.1016/j.commatsci.2021.110362

Machine Learning Prediction of Glass-Forming Ability in Bulk Metallic Glasses

Jie XIONG[b,c], San-Qiang SHI[b,c]*, Tong-Yi ZHANG[a,d]*

[a]School of Materials Science and Engineering, Harbin Institute of Technology, Shenzhen, China

[b]Department of Mechanical Engineering, The Hong Kong Polytechnic University, Hong Kong, China

[c]Shenzhen Research Institute, The Hong Kong Polytechnic University, Shenzhen, China

[d]Material Genome Institute, Shanghai University, Shanghai, China

Abstract

The critical casting diameter (D_{max}) quantitatively represents Glass-Forming Ability (GFA) of Bulk Metallic Glasses (BMGs). The present work constructed a dataset of two subsets, L-GFA subset of 376 BMGs with 1mm $\leq D_{max} <$ 5mm and G-GFA subset of 319 BMGs with $D_{max} \geq 5$ mm. The sequential backward selector and exhaustive feature selector are introduced to select key features. The trained XGBoost classifier with four selected features is able to successfully classify the L-GFA and G-GFA BMGs. Furthermore, the trained XGBoost regression model with another four selected features predicts the D_{max} of G-GFA samples with a cross-validated correlation coefficient of 0.8012. The correlation between features and D_{max} will provide the guidance in the design and discovery of novel BMGs.

Keywords: Machine Learning; XGBoost; Glass-Forming Ability; Bulk Metallic Glasses

1. Introduction

Bulk metallic glasses (BMGs) usually have outstanding mechanical and physical properties due to their amorphous structure. Glass-forming ability (GFA)[1,2] represents the ability of an alloy to form the amorphous structure at a given cooling rate and GFA can be quantitatively measured by the critical casting diameter D_{max}, below which an alloy is formed BMG and beyond which the alloy will be crystallized. Under the same casting condition, the larger the critical casting diameter of a BMG is, the higher the BMG GFA will be. The GFA of a BMG is the essential and fundamental feature and fully determined by the chemical composition of the BMG. Therefore, understanding and building-up the relationship between GFA and composition is

vital to the design and discovery of novel BMGs. The composition-space, however, is extremely large, which makes it greatly challenging to understand and build-up the relationship. Thus, other thermodynamic properties of BMGs, such as characteristic temperatures[3–7] of the glass transition temperature T_g, the onset crystallization temperature T_x, and the liquidus temperature T_l, which depend on chemical composition and have a feature-space much smaller than the composition-space, are widely used in the establishment of a GFA criterion of BMGs. Various combinations of the three characteristic temperatures are proposed to predict the critical casting diameter (D_{max}) and the correlation coefficient (r) of those predictions of D_{max} [8,9] is less than 0.56. In addition to the development of analytic formula of GFA criterion, the data-driven machine learning (ML) has recently been grown quickly to predict BMG GFA. For instance, Mastropietro et al. [10] utilized the linear regression and XGBoost algorithm to predict the maximum amorphous diameter of Fe-based BMGs. Ward et al.[11] developed random forest (RF) models built on a dataset comprising 6315 unique alloys to search BMGs from 2,711,547 candidates, six BMGs were experimentally found under the guidance of ML results. Ren et al.[12] employed adaptive ML based on the iteration of RF ML and experiments. The RF model was trained on available experimental results to suggest new experiments, and the new experimental results were added to the dataset to train the ML model again, and so on in iteration until reaching the goal. The adaptive ML discovered three metallic glass systems. Xiong et al.[8] used RF and symbolic regression (SR) to develop ML models for the prediction of GFA. The predictions of the RF model on unseen data were in good agreement with experimental results and the mathematical expression given by SR suggested three rules regarding the formation of BMGs. The ML models [8,10,11] predicted the D_{max} with an r value higher than 0.80, which is much better the conventional GFA criteria.

The previous ML classifications [8, 11] focus on the three classes of crystalline alloys, ribbon metallic glasses, and bulk metallic glasses and use the three classes to characterize GFA, and therefore less percentage of BMG data is both datasets in [8,11]. It is well-known that the mathematic basis of ML is probability and statistics, where data play the critical role. The present work investigates only BMG data generated from the most common technique, copper-mold casting, in order to avoid any potential influence from sample fabrication techniques. To distinguish ribbon metallic glasses from BMGs, the critical casting diameter of BMG should be higher than 1 mm, because the thickness of ribbon metallic glasses is at the sub-mm scale. With such considerations, the present work constructed a dataset containing 695 BMG samples (see Appendix I) with D_{max} ranging from 1 mm to 40 mm, among which 626 samples were

selected from the previous work [8], and other 69 samples with D_{max} greater than 5mm were collected from review articles [13–15]. The dataset is divided into two subsets, L-GFA subset of 376 BMGs with 1mm ≤D_{max} < 5mm and G-GFA subset of 319 BMGs with D_{max} ≥ 5 mm. Classification will be conducted on the data to classify the two groups of BMGs and regression will be done only on the G-GFA subset in order to predict the D_{max} values of BMGs more accurately.

The present work aimed at the development of ML models to predict the GFA of BMGs and thus a few of ML algorithms were adopted initially. The results show that the XGBoost algorithms in both classification and regression have stronger predictive power than other initially used ML algorithms.

2. Methodology

2.1 Data representation

In general, constituent elements of BMGs can be directly used as features, as did in [10], and atomic and electronic properties of constituent elements can also be used as features. The advantage by using atomic and electronic properties lies in the generalization of ML models, which maintains the atomic and electronic features and allows the change in constituent elements. Therefore, we utilize general-purpose features [16] in this work. The original twenty-five features are suggested and compiled with the average basic elemental property ($\bar{x}$) of constituent elements, the mismatch (δ_x) in elemental properties of constituent elements, the average atomic volume (V_a) [17] , the enthalpy (H_{mix}) and entropy (S_{mix}) of mixing [18], as defined by:

$$\bar{x} = \sum a_i \, x_i \tag{1}$$

$$\delta_x = \sqrt{\sum a_i \left(1 - \frac{x_i}{\bar{x}}\right)^2} \tag{2}$$

$$V_a = \sum a_i \cdot \frac{4}{3}\pi \cdot (R_m)_i^3 \tag{3}$$

$$H_{\mathrm{mix}} = 4 \sum_{j=i}^{N} \sum_{i=1}^{N} \Delta H_{ij} a_i a_j \tag{4}$$

$$S_{mix} = -R\sum_{i=1}^{N} a_i ln\, a_i \quad (5)$$

where a_i and x_i are the atomic fraction and elemental properties (shown in Table 1) of the i-th constituent element, respectively, ΔH_{ij} is the molar mixing enthalpy for binary liquid alloys[18], R is the gas constant. All features are scaled to [0, 1] for feature selection and model construction. According the value of D_{max}, the present work divides BMGs into two groups, one group has limited glass-forming ability (labeled as L-GFA) $D_{max} < 5$ and the other group has good GFA (labeled as G-GFA), i.e., $D_{max} \geq 5$ mm [19]. The constructed dataset comprises 376 L-GFA samples and 319 G-GFA samples.

Table 1. The used 11 basic elemental properties and their values were given in reference [8].

Elemental Property (Abbreviation)		
Metallic Radius (*Rm*)	Electron Affinity (*Eea*)	Mulliken Electronegativity (*Xm*)
Pauling Electronegativity (*Xp*)	Heat of Fusion (*Hf*)	First Ionization Potential (*I1*)
Second Ionization Potential (*I2*)	Melting Point (*Tm*)	Specific Heat Capacity (*Cp*)
Thermal Conductivity (*K*)	Valence Electrons (*VEC*)	

2.2 Feature selection

Two wrapper feature selection approaches, sequential backward selector (SBS) [20] and exhaustive feature selector (EFS) [20], are utilized in combination of seven ML algorithms. The SBS starts from the full set of N features and sequentially removes the least important features until reaching the minimum of a loss function, which yields the selected n features. The EFS is a brute-force approach and evaluates all possible feature combinations C_N^n to select the best subset. In the present work, the SBS is utilized first to determine an acceptable size of feature subset, and the EFS will evaluate the performance of all subsets have the determined size to search the best one.

2.3 Validation method

Ten-fold cross-validation (CV) is used in the present work, where the whole data are randomly and equally split into ten folds, nine folds form the training set and one fold forms the testing set. A ML model is trained on the training set and tested on the testing set. This process is repeated ten times, and the validation performance is obtained by the mean of the ten testing results [21]. The validation performance can be regarded as an estimation of the generalization

ability [22].

2.4 Performance metric

The performances of classification and regression models, respectively, are evaluated by the accuracy (*acc*) and coefficient of determination (R^2) in python library scikit-learn [21]. In addition, correlation coefficient (*r*), is also employed in this work to evaluate the performance of regression models. Their definitions are given below.

$$acc = \frac{T}{T+F} \tag{6}$$

$$R^2 = 1 - \frac{\sum_{i=1}^{n}(y_i - \hat{y}_i)^2}{\sum_{i=1}^{n}(y_i - \bar{y})^2} \tag{7}$$

$$r = \sqrt{\frac{\sum_{i=1}^{n}(\hat{y}_i - \bar{y})^2}{\sum_{i=1}^{n}(y_i - \bar{y})^2}} \tag{8}$$

where T and F stands for the number of correctly classified and wrongly classified samples, respectively. y_i and $\hat{y}_i$ is the actual and corresponding predicted value, and $\bar{y}$ is the mean of actual values. The value of *r* ranges from 0 to 1, 1 indicates a perfect fitting. It should be noticed that R^2 is not the square of *r*, an R^2 value of 1 indicates a perfect fitting and a negative value of R^2 indicates a very poor fitting.

3. Results and Discussion

3.1 Classification results

Support vector classifier with a linear function kernel (SVC-lin) and a radial basis function kernel (SVC-rbf), multi-layer perceptron classifier (MLPC), *k*-nearest neighbor classifier (KKNC), decision tree classifier (DTC), random forest classifier (RFC), and extreme gradient boosting classifier (XGBC) are used to distinguish L-GFA and G-GFA BMGs. All hyperparameters (HPs) of the above classifiers are set to the default values. The SBS is wrapped with the above seven algorithms to achieve an optimal combination of features and ML algorithms. Fig.1a shows the SBS results, indicating that XGBC and RFC models outperform other models. The SBS wrapped with XGBC (SBS-XGBC) gives a subset containing 12 features with a CV-*acc* value of 0.8518. To further reduce the feature number, the present work uses the 2% tolerance of CV-*acc* to balance the performance and the model complexity. Fig.1b shows the line of 2% tolerance and thus four features are determined, as shown in Table 2 with

associated values of CV-*acc*. Then, the EFS wrapped with XGBC and RFC, termed as EFS-RFC and EFS-XGBC, was conducted to search for the best one of the feature subset with four features from 12650 subset candidates and the results are also listed in Table 2 with associated values of CV-*acc*. Clearly, the EFS-RFC and EFS-XGBC select the four features slightly different from the four features of SBS-XGBC and SBS-RFC, respectively. The CV-*acc* values from the EFS-XGBC and EFS-RFC models are 0.8490 and 0.8460, respectively, better than those from SBS-XGBC and SBS-RFC models. After tuning hyperparameters with grid searches (see Appendix II for details), the EFS-XGBC and EFS-RFC model, yields a CV-*acc* value of 0.8561 and 0.8460, respectively.

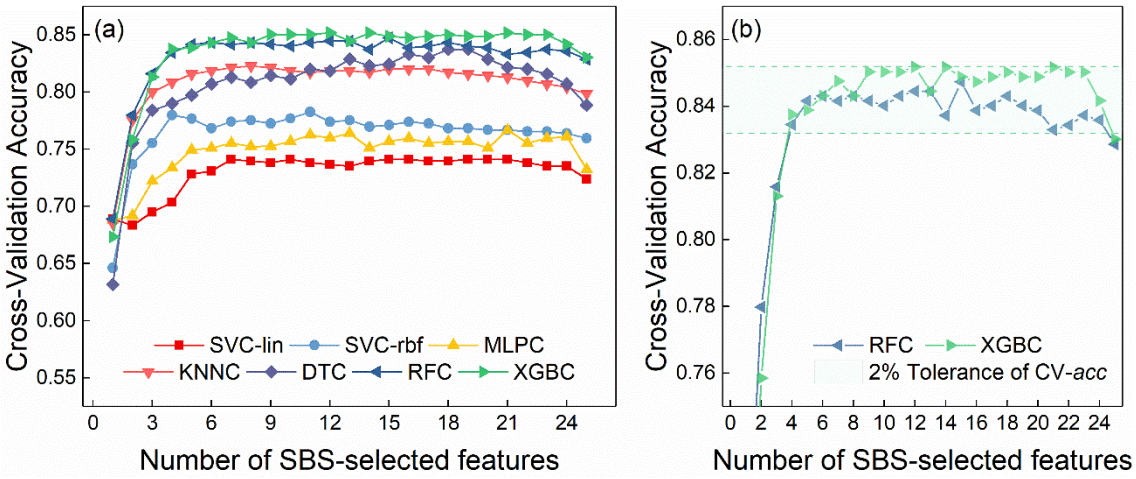

Fig.1 (a) The cross validated accuracy of the seven ML classifiers applied to different number of features selected by SBS approach. (b) The cross validated accuracy of the RFC and XGBC models built on various feature subsets

Table 2. Four features selected via SBS-RFC, SBS-XGBC, EFS-RFC, and EFS-XGBC algorithms.

ML Algorithms	Selected Features	Training *acc* (initial HPs)	CV-*acc* (initial HPs)	Training acc (tuned HPs)	CV-acc (tuned HPs)
SBS-RFC	δ_{Hf}, $\bar{I}1$, δ_{VEC}, S_{mix}	1.0	0.8346		
SBS-XGBC	δ_{Eea}, δ_{Xp}, δ_{Hf}, S_{mix}	1.0	0.8376		
EFS-RFC	$\overline{Eea}$, δ_{Xp}, δ_{Hf}, S_{mix}	1.0	0.8460	1.0	0.8460
EFS-XGBC	$\overline{Rm}$, δ_{Eea}, $\overline{Hf}$, S_{mix}	1.0	0.8490	1.0	0.8561

The detailed classification results are shown in Fig.2a confusion matrix of the EFS-XGBC with cross-validation. In a confusion matrix, all samples can be categorized as true

positive (TP), true negative (TN), false positive (FP), and false negative (FN). The precision and recall are defined by equations (9) and equations (10), respectively. In general, there exists a precision-recall conflict in classification, an ML model often reduces recall with improving precision and vice versa. The F_1 score defined by equation (11) is the harmonic mean of precision and recall. The EFS-XGBC model gives the F_1 scores of 0.8450 and 0.8656 for G-GFA and L-GFA class, respectively. Fig.2b shows the G-GFA receiver operating characteristic (ROC) curve, which is the curve of the true positive rate (TPR = recall) against the false positive rate (FPR). The area under the G-GFA ROC curve is 0.9045, indicating the outstanding classification of the ML model [23].

$$precision = \frac{TP}{TP + FP} \tag{9}$$

$$recall = \frac{TP}{TP + FN} \tag{10}$$

$$F_1\ score = 2 \cdot \frac{precision \cdot recall}{precision + recall} \tag{11}$$

$$FPR = \frac{FP}{FP + TN} \tag{12}$$

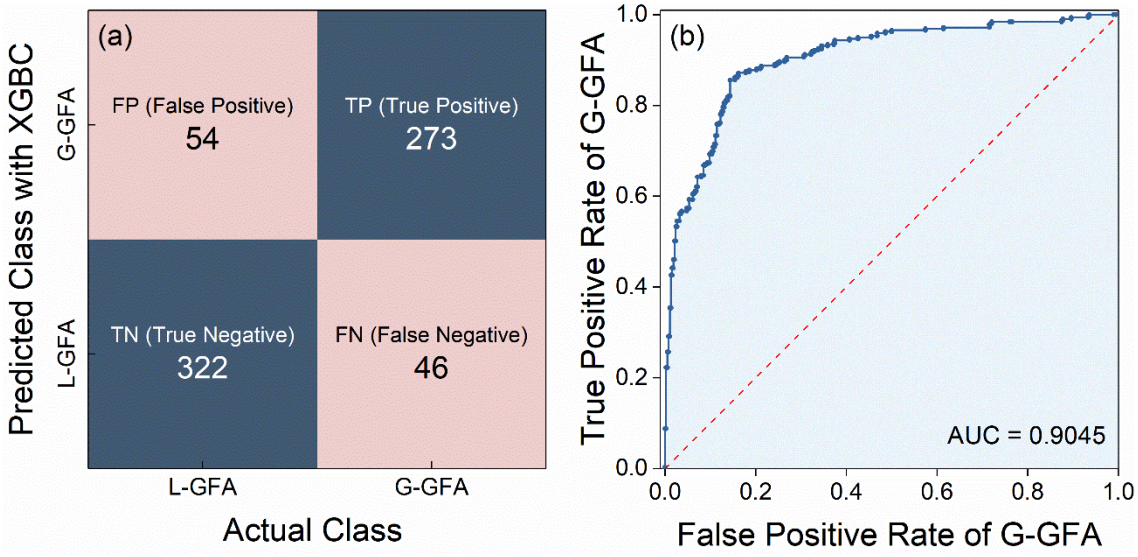

Fig.2 (a) The confusion matrix of classifying the GFA of BMGs and (b) the receiver operating characteristic (ROC) curve for the G-GFA class using the EFS-XGBC model under cross-validation.

3.2 Regression results

The support vector regressor with a linear function kernel (SVR-lin) and a radial basis function

kernel (SVR-rbf), multi-layer perceptron regressor (MLPR), *k*-nearest neighbor regressor (KKNR), decision tree regressor (DTR), random forest regressor (RFR), and extreme gradient boosting regressor (XGBR) were conducted on the G-GFA BMGs dataset and all hyperparameters are initially set to the default values, except for the *max_features* setting of 1/3 in RFR.

Table 3. Four features selected via EFS-RFR, and EFS-XGBR.

ML Algorithms	Selected Features	Training R^2 (initial HPs)	CV-R^2 (initial HPs)	Training R^2 (tuned HPs)	CV-R^2 (tuned HPs)
RFR	$\overline{Xp}$, δ_{Hf}, δ_{I2}, δ_K	0.9774	0.5984	0.9774	0.6011
XGBR	δ_{Rm}, δ_{Hf}, $\overline{Tm}$, δ_{Cm}	0.9999	0.5846	0.9994	0.6193

Fig.3a indicates that the SBS-RFR and SBS-XGBR models perform much better than other SBS-ML models. The SBS-RFR model finds a feature subset containing seven features with a CV-R^2 value of 0.6079, as shown in Fig.3b. The 2% tolerance of CV-R^2 reduces further the feature number to four. Table 3 lists the selected best feature subsets from EFS-RFR and EFS-XGBR and the associated values of CV-R^2. After tuning hyperparameters (see Appendix II for details), the CV-R^2 values of EFS-RFR and EFS-XGBR models are 0.6011 and 0.6193, respectively, as shown in Table 3. Thus, the EFS-XGBR model is used in the following analysis.

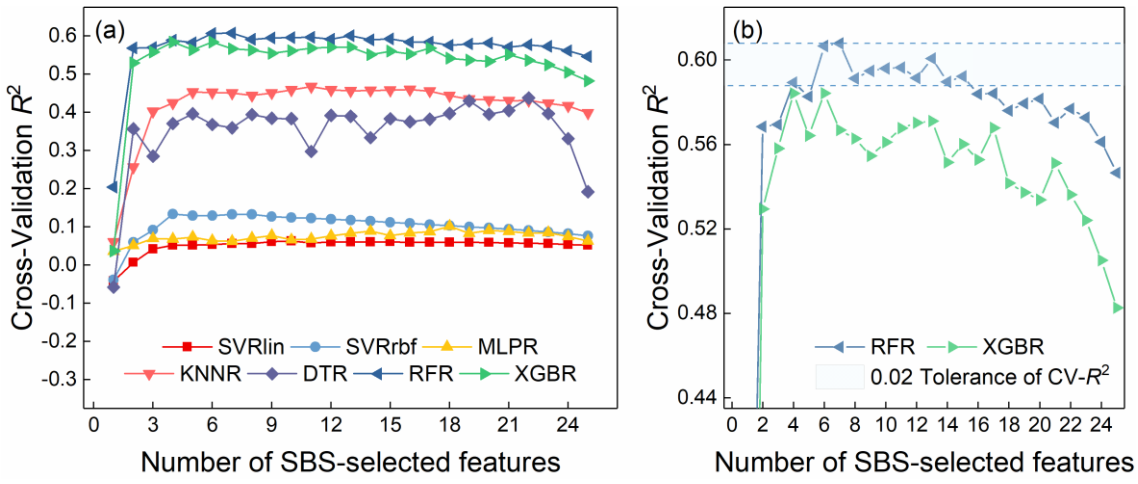

Fig.3 (a) The cross validated R^2 of seven ML regression algorithms applied to different number of features selected by SBS approach. (b) The cross validated R^2 of the RFR and XGBR models built on various feature subsets

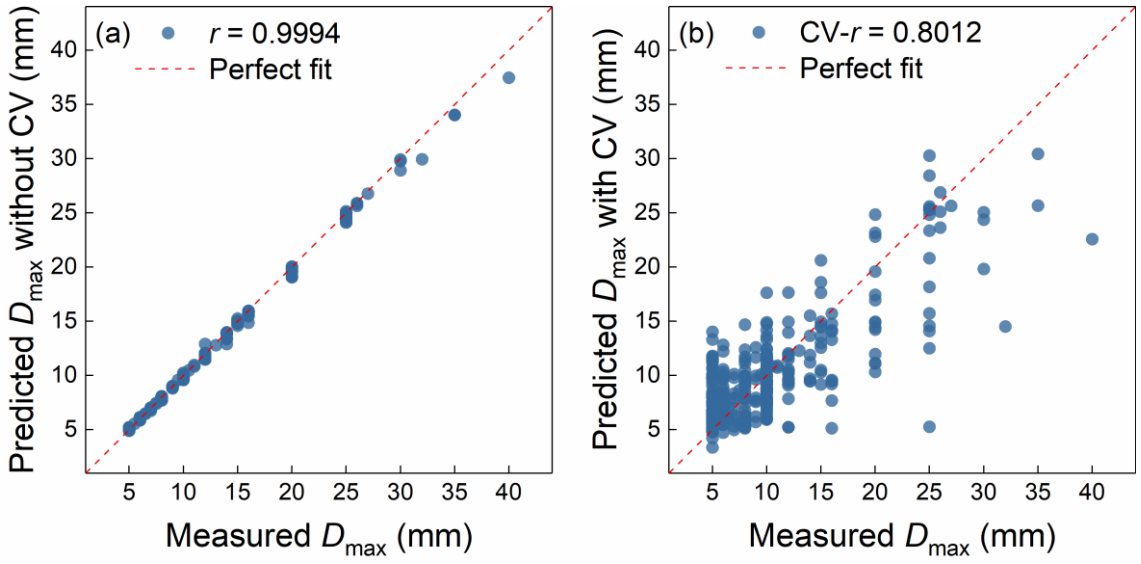

Fig.4 The predicted D_{max} values with EFS-XGBR model are plotted against the corresponding values (a) without and (b) with cross-validation.

Fig.4(a, b) shows the measured D_{max} values versus the predicted values on the training data set and the testing set, respectively. As expected, the prediction of the EFS-XGBR model on the training set has an extremely high *r* value of 0.9994, meaning that the model is perfectly trained, and the CV-*r* value remains 0.8012 under the validation. We recalculate the CV-*r* value of the reported ML models [8,11] on the D_{max} prediction with all alloy data sets and just BMG datasets. As shown in Table 4, the present EFS-XGBR model with only four features performs over the other two RFR models with more features [8,11].

Table 4. The performances of three ML models in the D_{max} prediction.

ML algorithm	CV-*r* on predicting D_{max}	Number of Features	reference
RFR	0.85 (all alloys) / 0.7368 (BMGs)	6	[8]
RFR	0.89 (all alloys) / 0.8000 (BMGs)	210	[11]
XGBR	0.8012 (BMGs)	4	This work

3.3 Feature Importance

The XGBoost algorithm can calculate the feature importance during the model construction. Figs.5(a, b) show the feature importance for XGBoost classification and regression,

respectively. The XGBC model ranks $\overline{Rm}$ as top one in the feature importance, followed by $\overline{Hf}$, S_{mix}, and δ_{Eea}. The $\overline{Rm}$ influences atomic packing efficiency, which may significantly affect the GFA of BMGs [24]. The features $\overline{Hf}$ [14] and S_{mix} [8] are reported to play important roles in the GFA of BMGs. The feature δ_{Eea} reflects the atomic size difference (δ_{Rm}) and thus influences GFA as well. The XGBR model puts δ_{Hf} at the top of feature importance and then $\overline{Tm}$, δ_{Cm}, and δ_{Rm} in sequence. The features δ_{Hf}, δ_{Cm}, and δ_{Rm} represent the mismatch in elemental properties and infer the uniformity between components [25], and thus affect the GFA. The feature $\overline{Tm}$ is an estimator of the melting temperature of BMGs, which will affect the crystallization of BMGs and thus plays an important role in GFA [8,26].

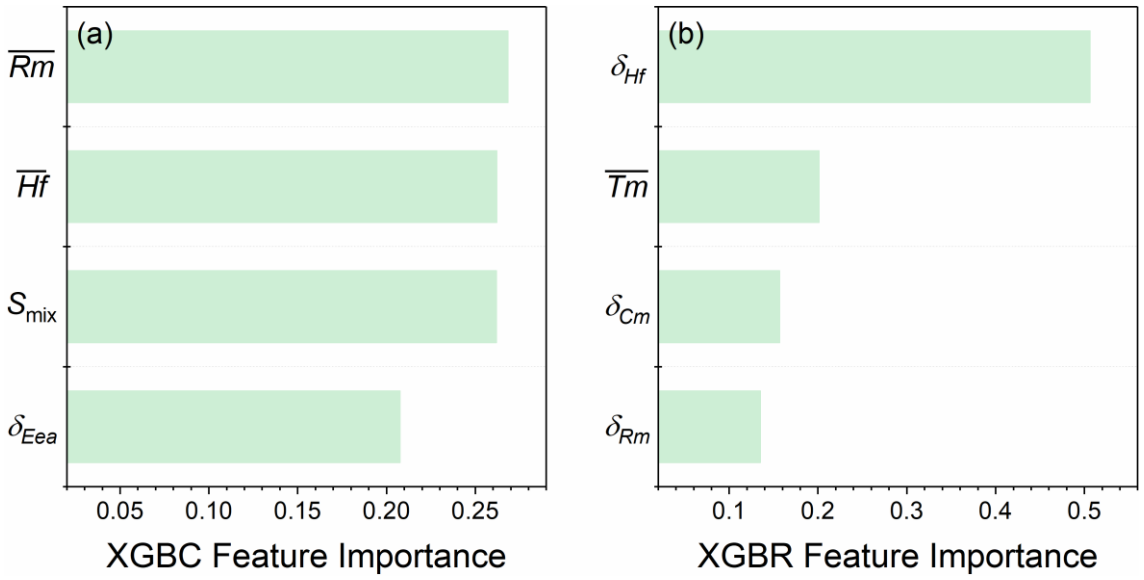

Fig.5 The feature importance of selected features for (a) classification and (b) regression based on the XGBoost algorithm.

3.4 Generalization Capability of the Built Models

To demonstrate the generalization capability of the built XGBC model, the model is applied on the data of 1552 crystalline alloys (CRA) and 3708 ribbon metallic glasses (RMG) in reference [8]. The classification results are shown in the confusion matrix of Fig. 6(a), indicating that the XGBC model can successfully distinguish G-GFA alloys from non-G-GFA alloys (crystalline alloys, ribbon metallic glasses, and L-GFA BMGs).

Since Cu- and Zr- based BMGs are promising engineering materials due to their good GFA and excellent mechanical properties [27], we will use the built XGBC and XGBS models to discover novel BMGs in the search space of 381 potential $(AgAl)_xCu_yZr_z$ BMGs, where Ag

and Al atomic fractions are in the range of $5\% \le x \le 8\%$ varying in a step of 1%, and y and z vary in the step of 0.5% within $y \ge 20\%$ and $z \ge 20\%$ under the constraint of $x + y + z = 100\%$. Firstly, the XGBC model identifies 239 G-GFA BMGs from the search space. Then, the built XGBS model predicts the D_{max}-values of the G-GFA BMGs classified by the built XGBC model. Fig.6(b) shows the good agreement between the ML predictions and the available experimental results [28] and the Zr-rich Ag-Al-Cu-Zr BMGs have generally greater D_{max} than the Cu-rich Ag-Al-Cu-Zr BMGs. In addition, a novel BMG $Zr_{48.5}Cu_{35.5}Ag_8Al_8$ with 22.2 mm D_{max} is discovered via the built ML models.

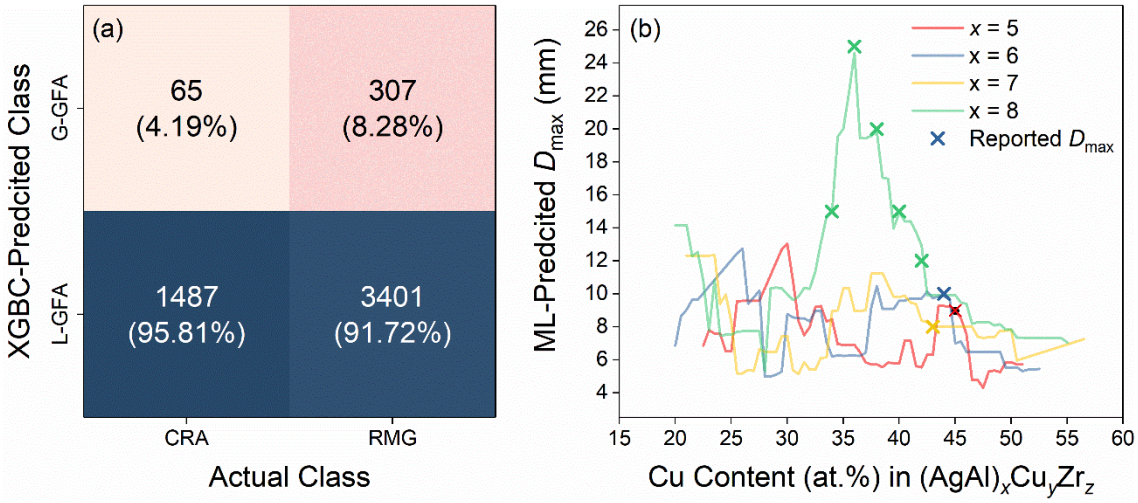

Fig.6 (a) The confusion matrix of EFS-XGBC model on 1552 crystalline alloys (CRA) and 3708 ribbon metallic glasses (RMG). (b) The predicted D_{max} values with EFS-XGBR model of $(AgAl)_xCu_yZr_z$ glassy alloys, the reported values are marked as crosses.

Conclusions

This work conducted the seven ML algorithms to predict the GFA and D_{max} of BMGs based on the copper-mold casting 695 data. The feature selection was conducted using different ML algorithms to select the optimal combination of ML algorithm and features. The results indicate that XGBoost outperforms the other used ML algorithms. The XGBC model with four features of $\overline{Rm}$, δ_{Eea}, $\overline{Hf}$, and S_{mix} can successfully classify L-GFA and G-GFA BMGs with the CV-*acc* of 0.8561. The XGBR model with four features of δ_{Rm}, δ_{Hf}, $\overline{Tm}$, and δ_{Cm} predicts the D_{max} value of G-GFA BMGs with the CV-*r* value of 0.8012.

Data Availability

All ML approaches are performed on Python. The SBS and EFS algorithms are available in Mlxtend libraries, the XGBoost algorithms are performed by the XGBoost library, and other algorithms are available in scikit-learn libraries. The raw data required to reproduce these findings are available from the corresponding author on request.

Acknowledgments

This work was supported by the National Key Research and Development Program of China (No. 2018YFB0704400), the Hong Kong Polytechnic University (internal grant Nos. 1-ZE8R and G-YBDH), and the 111 Project (grant No. D16002) from the State Administration of Foreign Experts Affairs, PRC.

Reference

[1] K.C. Chan, J. Sort, Metallic Glasses, Metals (Basel). 1 (2014) 305–385. doi:10.1016/B978-0-444-53770-6.00004-6.

[2] W.H. Wang, The elastic properties, elastic models and elastic perspectives of metallic glasses, Prog Mater Sci. 57 (2012) 487–656. doi:10.1016/j.pmatsci.2011.07.001.

[3] B.S. Dong, S.X. Zhou, D.R. Li, C.W. Lu, F. Guo, X.J. Ni, Z.C. Lu, A new criterion for predicting glass forming ability of bulk metallic glasses and some critical discussions, Prog Nat Sci Mater Int. 21 (2011) 164–172. doi:10.1016/S1002-0071(12)60051-3.

[4] X.H. Du, J.C. Huang, New criterion in predicting glass forming ability of various glass-forming systems, Chinese Phys B. 17 (2008) 249–254. doi:Doi 10.1088/1674-1056/17/1/043.

[5] Q.J. Chen, J. Shen, D.L. Zhang, H.B. Fan, J. Sun, D.G. McCartney, A new criterion for evaluating the glass-forming ability of bulk metallic glasses, Mater Sci Eng A-Structural Mater Prop Microstruct Process. 433 (2006) 155–160. doi:10.1016/j.msea.2006.06.053.

[6] A. Inoue, Stabilization of metallic supercooled liquid and bulk amorphous alloys, Acta Mater. 48 (2000) 279–306. doi:Doi 10.1016/S1359-6454(99)00300-6.

[7] Z.P. Lu, Y. Li, S.C. Ng, Reduced glass transition temperature and glass forming ability of bulk glass forming alloys, J Non Cryst Solids. 270 (2000) 103–114. doi:Doi 10.1016/S0022-3093(00)00064-8.

[8] J. Xiong, S.Q. Shi, T.Y. Zhang, A machine-learning approach to predicting and understanding the properties of amorphous metallic alloys, Mater Des. (2020). doi:10.1016/j.matdes.2019.108378.

[9] J. Xiong, T.Y. Zhang, S.Q. Shi, Machine learning prediction of elastic properties and glass-forming ability of bulk metallic glasses, Mrs Commun. 9 (2019) 576–585. doi:10.1557/mrc.2019.44.

[10] D.G. Mastropietro, J.A. Moya, Design of Fe-based bulk metallic glasses for maximum amorphous diameter (Dmax) using machine learning models, Comput Mater Sci. (2021). doi:10.1016/j.commatsci.2020.110230.

[11] L. Ward, S.C. O'Keeffe, J. Stevick, G.R. Jelbert, M. Aykol, C. Wolverton, A machine learning approach for engineering bulk metallic glass alloys, Acta Mater. 159 (2018) 102–111. doi:10.1016/j.actamat.2018.08.002.

[12] F. Ren, L. Ward, T. Williams, K.J. Laws, C. Wolverton, J. Hattrick-Simpers, A. Mehta, Accelerated discovery of metallic glasses through iteration of machine learning and high-throughput experiments, Sci Adv. 4 (2018). doi:10.1126/sciadv.aaq1566.

[13] P. Gong, L. Deng, J. Jin, S. Wang, X. Wang, K. Yao, Review on the research and development of Ti-based bulk metallic glasses, Metals (Basel). (2016). doi:10.3390/met6110264.

[14] A.H. Cai, H. Chen, W.K. An, J.Y. Tan, Y. Zhou, Y. Pan, G.X. Sun, Melting enthalpy ΔHm for describing glass forming ability of bulk metallic glasses, J Non Cryst Solids. (2008). doi:10.1016/j.jnoncrysol.2007.08.066.

[15] Y. Li, S. Zhao, Y. Liu, P. Gong, J. Schroers, How Many Bulk Metallic Glasses Are There?, ACS Comb Sci. (2017). doi:10.1021/acscombsci.7b00048.

[16] L. Ward, A. Agrawal, A. Choudhary, C. Wolverton, A general-purpose machine learning framework for predicting properties of inorganic materials, Npj Comput Mater. 2 (2016) 16028. doi:10.1038/npjcompumats.2016.28.

[17] J.Q. Wang, W.H. Wang, H.B. Yu, H.Y. Bai, Correlations between elastic moduli and molar volume in metallic glasses, Appl Phys Lett. 94 (2009). doi:10.1063/1.3106110.

[18] P.K. Ray, M. Akinc, M.J. Kramer, Applications of an extended Miedema's model for ternary alloys, J Alloys Compd. 489 (2010) 357–361. doi:10.1016/j.jallcom.2009.07.062.

[19] J. Mei, Titanium-based Bulk Metallic Glasses : Glass Forming Ability and Mechanical Behavior, Northwestern Polytechnical University, 2010.

[20] S. Raschka, MLxtend: Providing machine learning and data science utilities and extensions to Python's scientific computing stack, J Open Source Softw. (2018). doi:10.21105/joss.00638.

[21] F. Pedregosa, G. Varoquaux, A. Gramfort, V. Michel, B. Thirion, O. Grisel, M. Blondel, P. Prettenhofer, R. Weiss, V. Dubourg, J. Vanderplas, A. Passos, D. Cournapeau, M. Brucher, M. Perrot, É. Duchesnay, Scikit-learn: Machine learning in Python, J Mach Learn Res. (2011).

[22] S. Arlot, A. Celisse, A survey of cross-validation procedures for model selection, Stat Surv. (2010). doi:10.1214/09-SS054.

[23] D.W. Hosmer, S. Lemeshow, Applied Logistic Regression, 2005. doi:10.1002/0471722146.

[24] K.J. Laws, K.F. Shamlaye, K. Wong, B. Gun, M. Ferry, Prediction of glass-forming compositions in metallic systems: Copper-based bulk metallic glasses in the Cu-Mg-Ca system, Metall Mater Trans A Phys Metall Mater Sci. 41 (2010) 1699–1705. doi:10.1007/s11661-010-0274-7.

[25] Y. Zhang, C. Wen, C. Wang, S. Antonov, D. Xue, Y. Bai, Y. Su, Phase prediction in high entropy alloys with a rational selection of materials descriptors and machine learning models, Acta Mater. (2020). doi:10.1016/j.actamat.2019.11.067.

[26] J.D. Hoffman, Thermodynamic driving force in nucleation and growth processes, J Chem Phys. (1958). doi:10.1063/1.1744688.

[27] H.-J. Fecht, H. Franz, Q.K. Jiang, X.D. Wang, H. Ma, G.Q. Zhang, J. Bendnarcik, Q.P. Cao, Y.G. Liu, J.Z. Jiang, X.P. Nie, Zr-(Cu,Ag)-Al bulk metallic glasses, Acta Mater. 56 (2008) 1785–1796. doi:10.1016/j.actamat.2007.12.030.

[28] W. Zhang, Q. Zhang, C. Qin, A. Inoue, Synthesis and properties of Cu-Zr-Ag-Al glassy alloys with high glass-forming ability, Mater Sci Eng B Solid-State Mater Adv Technol. 148 (2008) 92–96. doi:10.1016/j.mseb.2007.09.064.